ACS APPLIED MATERIALS & INTERFACES

Research Article

www.acsami.org

# Magnetic Affinity Microspheres with Meso-/Macroporous Shells for Selective Enrichment and Fast Separation of Phosphorylated Biomolecules

Gong Cheng,[†,∥] Zhi-Gang Wang,[†,∥] Yan-Lin Liu,[†,∥] Ji-Lin Zhang,*[,†] De-Hui Sun,[‡] and Jia-Zuan Ni[†,§]

[†]State Key Laboratory of Rare Earth Resource Utilization, Changchun Institute of Applied Chemistry, Chinese Academy of Sciences, Changchun 130022, China

[‡]Changchun Institute Technology, Changchun 130012, China

[§]College of Life Science, Shenzhen University, Shenzhen 518060, China

[∥]University of Chinese Academy of Sciences, Beijing 100049, China

Supporting Information

**ABSTRACT:** The flowerlike multifunctional affinity microspheres prepared by a facile solvothermal synthesis and subsequent calcination process consist of magnetic cores and hierarchical meso-/macroporous $TiO_2$ shells. The hierarchical porous structure of the flowerlike affinity microspheres is constructed by the macroporous shell from the stacked mesoporous nanopetals which are assembled by small crystallites. The affinity microspheres have a relatively large specific surface area of 50.45 $m^2\ g^{-1}$ and superparamagnetism with a saturation magnetization ($M_s$) value of 30.1 emu $g^{-1}$. We further demonstrate that they can be applied for rapid and effective purification of phosphoproteins, in virtue of their selective affinity, porous structure, and strong magnetism. In addition, the affinity microspheres can also be used for enrichment of phosphopeptides, and the selectivity is greatly improved due to the increase of mass transport and prevention of the possible "shadow effect" resulting from the smaller and deeper pores by taking advantage of the unique porous structure. Overall, this work will be highly beneficial for future applications in the isolation and identification of phosphorylated biomolecules.

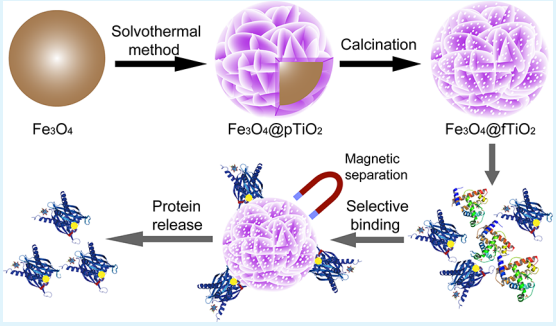


**KEYWORDS:** *affinity probe, porous structure, protein separation, peptide enrichment, biotechnology*

## INTRODCUTION

Multifunctional hierarchical architectures with designed structures, controlled morphologies, large surface area, and desirable components have fueled research on the construction of affinity probes and the interaction of biomolecules.[1−3] Hierarchical architectures with tailored textures would facilitate interaction between the affinity materials and target biomolecules because the unique chemical, physical, and surface properties of nanostructured materials may effectively contribute to shorten the biomolecule transfer-distance and provide an affinity-mediating function.[4−7] Especially, various metal oxide nanostructures have been demonstrated to be effective for selective separation and adsorption of biomolecules owing to their selective affinity, large specific surface area, and modifiable surface properties.[8−10] However, significant challenges remain in the development of affinity nanostructures that show large surface area, easy biomolecule transfer, superior specificity, and high sensitivity.

Protein phosphorylation is one of the most important post-translated modifications involved in regulating various cellular processes such as metabolism, signaling, cell growth, and division. It is reported that many diseases (e.g., cancer and Alzheimer) are relevant to the abnormal phosphorylation,[11,12] and some phosphoproteins and phosphopeptides play important roles in medical inspection.[13−15] Thus, the identification of phosphorylated biomolecules is a fundamental step toward understanding and detecting the signaling pathways in normal and disease states. Nevertheless, the detection of phosphorylated biomolecules remains a major challenge due to the small quantity of phosphoproteins, the low ratio of phosphorylation, and the signal suppression effect by nonphosphopeptides or proteins.[16,17] In recent years, significant efforts have been expended to the development of affinity materials that can rapidly and effectively enrich or isolate phosphopeptides,[18,19] and metal-ion immobilized and metal oxide materials are the most commonly used affinity materials.[20−24] Especially, mesoporous metal oxide nanostructures have been developed as affinity probes and represent current state of the art for selective capture of low-abundance phosphopeptides, due to their high surface area, superior

Received: January 16, 2013
Accepted: March 20, 2013
Published: March 20, 2013

  

chemicophysical behavior and excellent surface properties.[25,26] However, the "shadow effect" from the smaller and deeper pores would be unavoidable and hamper the release of target biomolecules.[27−30] Therefore, only a few of them can be applied for extraction of target peptides from the complex real biosamples. Furthermore, few of them could be used for purification of phosphoproteins, because the single-sized mesoporous materials often suffer from the size exclusion effect due to the relative large size of target proteins, resulting in the low adsorption efficiency and significant sample losses during the washing steps.[31−33] In addition, the centrifugal separation used for isolating the nanostructures carrying target biomolecules from complex biological samples is a time-consuming and inconvenient procedure. Considering the facile separation of magnetic particles under an external magnetic field, magnetic particles have been applied in bioseparation.[34−37]

Although some flowerlike $TiO_2$ microspheres with hierarchical structures were prepared via solvothermal/hydrothermal method using $TiCl_4$ or titanate as precursor and pure ethanol or isopropanol with organic additive (e.g., glycerol, glycine) as solvent,[38−41] little work has been carried out for the core−shell $Fe_3O_4$@$TiO_2$ microspheres with similar hierarchical flowerlike $TiO_2$ shell based on the above method.[42,43] For example, Li et al.[42] reported synthesis of the flowerlike $Fe_3O_4$@$TiO_2$ yolk-shell microspheres by means of $Fe_3O_4$@$SiO_2$@$TiO_2$ semi-finished product. Chen et al.[43] reported preparation of the flowerlike magnetic nanorattles by reducing the as-synthesized $\alpha$-$Fe_2O_3$@$TiO_2$−NS which was obtained via the solvothermal method using $\alpha$-$Fe_2O_3$@$SiO_2$@$SnO_2$ and titanium isopropoxide as precursors. By this token, it is difficult to directly coat the affinity shells with hierarchical porous structure on the surface of $Fe_3O_4$ particles. Herein, to address above issues, we report a facile fabrication of the flowerlike core/shell affinity microspheres with magnetic $Fe_3O_4$ cores and hierarchical meso-/macroporous $TiO_2$ shells (denoted as $Fe_3O_4$@f$TiO_2$) for selective enrichment and fast separation of phosphorylated biomolecules. Both the phosphoproteins and phosphopeptides can be effectively enriched, and the enrichment efficiency and selectivity were highly improved by taking advantage of the meso-/macroporous affinity structure for increasing mass transport of target biomolecules. Meanwhile, such porous structure holding the merit of large specific surface area can further increase adsorption efficiency and MS detection sensitivity of the phosphorylated proteins/peptides due to the more adsorption sites for target biomolecules. In addition, compared with the bioseparation techniques used frequently (e.g., filtration, ion exchange, centrifugation, and gravitational separation), the magnetic bioseparation technique with high efficiency and low cost can realize the fast, simple, and effective isolation of biosamples. It is expected that this work could provide new insights for the design of the affinity probes for extracting and separating low-abundance biomarkers from complex biosamples in biomedical applications.

## EXPERIMENTAL SECTION

**Chemicals.** Ferric chloride ($FeCl_3·6H_2O$), ethylene glycol (EG), isopropanol (IPA), dimethylformamide (DMF), and ammonium hydroxide ($NH_3·H_2O$) were obtained from Beijing Chemical Regent Co., Ltd. (Beijing, China). Tetrabutyl titanate (TBOT), trifluoroacetic acid (TFA), acetonitrile (ACN), ammonium bicarbonate ($NH_4HCO_3$), sinapic acid (SA), 2,5-dihydroxybenzoic acid (2,5-DHB), and dithiothreitol (DTT) were purchased from Aladdin (Shanghai, China). Bovine $\beta$-casein, bovine serum albumin (BSA), myoglobin (from equine heart), horseradish peroxidase, and trypsin (from bovine pancreas, TPCK treated) were purchased from Sigma-Aldrich (St. Louis, MO, USA). Iodoacetamide (IAA) was provided by Alfa Aesar (USA).

**Preparation of Core/Shell Structured $Fe_3O_4$@f$TiO_2$ Microspheres.** The magnetic $Fe_3O_4$ particles were prepared according to our previous reported synthetic process.[44] Typically, $FeCl_3·6H_2O$ (2.72 g) and NaAc (7.20 g) were completely dissolved in EG (80 mL) under vigorously magnetic stirring. The obtained homogeneous solution was transferred to a Teflon-lined stainless-steel autoclave (120 mL) and sealed to heat at 180 °C for 6 h. Then, it was cooled to room temperature naturally. The obtained product was washed with ethanol and deionized water in sequence with the help of a magnet and, then, dried in vacuum at 60 °C for 12 h.

The flowerlike $Fe_3O_4$@f$TiO_2$ hierarchical microspheres were synthesized by a facile solvothermal method. Typically, the as-synthesized $Fe_3O_4$ particles (40 mg; see Figure S1) were fully dispersed in DMF (10 mL) and IPA (30 mL) under ultrasonication. Then, TBOT (2 mL) was added to the above dispersion with ultrasonic treatment for 5 min. The mixture was transferred into a Teflon-lined stainless steel autoclave (50 mL) and heated to 200 °C for 10 h. Finally, the products were washed with ethanol, dried overnight at 60 °C, and calcined at 400 °C for 2 h.

**Characterization of $Fe_3O_4$@f$TiO_2$ Microspheres.** A field emission scanning electron microscope (FESEM, S4800, Hitachi) equipped with an energy-dispersive X-ray spectrum (EDX, JEOLJXA-840) was applied to determine morphologies and compositions of the as-prepared samples. Transmission electron microscopy (TEM) and high-resolution TEM (HRTEM) images were taken with a FEI Tecnai G2 S-Twin transmission electron microscope operated at 200 kV. Powder X-ray diffraction (XRD) patterns were collected on a Bruker D8 Focus X-ray diffractometer using Cu K$\alpha$ radiation ($\lambda$ = 1.5405 Å). Fourier-transform infrared spectroscopy (FTIR) analysis was carried out on a Perkin-Elmer 580B infrared spectrophotometer using the KBr pellet technique. Nitrogen adsorption isotherms were measured at a liquid nitrogen temperature (77 K) with a Micromeritcs ASAP 2010 M apparatus. The specific surface area was determined by the Brunauer−Emmett−Teller (BET) method. The total pore volume was evaluated by the *t*-plot method, and pore size distribution was analyzed with the supplied BJH software package from the adsorption branch of the isotherms. Magnetization measurement was carried out with a superconducting quantum interface device (SQUID) magnetometer (Quantum Design MPMS XL) at 300 K.

**Purification of Phosphoproteins.** To evaluate selectivity and efficiency of the $Fe_3O_4$@f$TiO_2$ microspheres for enrichment of phosphoproteins, the $Fe_3O_4$@f$TiO_2$ microspheres (3 mg) were incubated in a phosphoprotein ($\beta$-casein) solution with different concentration (3 mL buffer solution containing 50% acetonitrile and 0.5% TFA) with shaking. After adsorption, the $Fe_3O_4$@f$TiO_2$ microspheres captured phosphoproteins were isolated from the suspension with a magnet. The concentrations of residual proteins in the supernatant were detected, and the adsorption capacities were calculated indirectly. The collected supernatant was lyophilized to dryness and subsequently dissolved in PBS solution. The resulting protein solution was measured using a UV−visible absorption spectrophotometer under monitored at 280 nm. The UV−vis absorption spectroscopy analysis was carried out with a Shimadzu UV-1750 UV−visible spectrophotometer.

To further evaluate selectivity and efficiency of the $Fe_3O_4$@f$TiO_2$ microspheres for enrichment of phosphoproteins, a complex protein solution (prepared in the 50% acetonitrile and 0.5% TFA buffer solution) containing $\beta$-casein ($1 \times 10^{-7}$ M), myoglobin ($2 \times 10^{-7}$ M), horseradish peroxidase ($1 \times 10^{-6}$ M), and BSA ($2.5 \times 10^{-5}$ M) was used. $Fe_3O_4$@f$TiO_2$ microspheres (0.2 mg) were incubated in 60 $\mu$L of the protein mixture solution with shaking for 30 min. The $Fe_3O_4$@f$TiO_2$ microspheres were isolated from the suspension with a magnet and, then, washed with the buffer solution two times. To elute the captured proteins, the $Fe_3O_4$@f$TiO_2$ microspheres were redispersed into 40 $\mu$L of 10% ammonium hydroxide with shaking for 5 min. After

magnetic separation, the supernatant was collected and lyophilized to dryness. According to the same procedure, the controlling test was performed using commercial $TiO_2$ particles as the substitute of the $Fe_3O_4$@f$TiO_2$ microspheres.

**Selective Enrichment of Phosphopeptides.** To evaluate selectivity and practice service performance of the $Fe_3O_4$@f$TiO_2$ microspheres for enrichment of phosphopeptides, the digests of $\beta$-casein and BSA were used as the complex peptide testing solutions. A 1.0 mg portin of $\beta$-casein or BSA was dissolved in 1 mL of 50 mM $NH_4HCO_3$ solution. Then, trypsin was added into the solution with a ratio of 50:1 (protein/trypsin, w/w). After that, the solution was incubated at 37 °C for 16 h. Finally, the obtained tryptic digests were diluted to the target concentration with 0.5% TFA solution in acetonitrile/deionized water (1/1, v/v).

Enrichment experiments of the phosphopeptides are described as follows. A 100 $\mu$L portion of protein digest solution was mixed with 5 $\mu$L of 20 mg/mL $Fe_3O_4$@f$TiO_2$ microspheres suspending solution and then shaken for 2 min. Subsequently, the microspheres captured phosphopeptides were collected and isolated from the mixture with the help of a magnet. The obtained microspheres were washed with 50 $\mu$L 0.5% TFA solution in acetonitrile/deionized water (1/1, v/v) three times. For the peptide mixture of $\beta$-casein and BSA, three aqueous solutions of 0.5%, 1.0%, or 1.5% TFA in acetonitrile/deionized water (1/1, v/v) were used to optimize the affinity selectivity. After that, the trapped phosphopeptides were eluted with 20 $\mu$L of 10% ammonium hydroxide. After magnetic separation, the supernatant was collected and lyophilized to dryness.

For enriching and isolating the phosphopeptides from human serum, the pristine human serum (0.5 $\mu$L) used as the real sample was dissolved in 50 $\mu$L 0.5% TFA solution in acetonitrile/deionized water (1/1, v/v) and, then, treated according to the same procedure as the standard protein digests.

**Mass Spectrometry Analysis.** Matrix-assisted laser desorption/ionization time-of-flight mass spectrometry (MALDI-TOF MS) analysis. The above products obtained from the elution step were dissolved in 2 $\mu$L of matrix solution containing 20 mg/mL SA (for proteins) or DHB (for peptides) in 50% acetonitrile and 1% $H_3PO_4$ aqueous solution (v/v) by pipetting, and 0.5 $\mu$L of the mixture was deposited onto the MALDI target. MALDI-TOF MS experiment were performed on Bruker Autoflex III MALDI-TOF MS (Bruker Daltonics Bremen, Germany) equipped with a 355-nm Nd:YAG laser. The acceleration voltage and repetition rate were set at 19 kV and 200 Hz, respectively, while the laser power was optimized. MS spectra were acquired as an average of 100 laser shots for three times, which was obtained in positive ion reflection mode and analyzed by Bruker Daltonics flex Analysis software.

## RESULTS AND DISCUSSION

The morphologies, elemental analysis, crystal and surface structures, and magnetism of the flowerlike $Fe_3O_4$@f$TiO_2$ microspheres were characterized using modern testing instruments. A possible formation mechanism is proposed based on time-dependent evolution experiments. The selectivity and efficiency of the $Fe_3O_4$@f$TiO_2$ microspheres for phosphorylated protein/peptide separation were evaluated using a commercial phosphoprotein ($\beta$-casein) and a normal protein (BSA) as model proteins. Finally, the affinity microspheres were applied to enrich phosphopeptides from the real biological sample (the pristine human serum).

**Morphologies and Structures of the Flowerlike $Fe_3O_4$@f$TiO_2$ Microspheres.** As illustrated in Scheme 1a, the hierarchical flowerlike $Fe_3O_4$@f$TiO_2$ microspheres were synthesized by a facile solvothermal synthesis and subsequent calcination process. The flowerlike precursor composites with macroporous shell (denoted as $Fe_3O_4$@p$TiO_2$) were first prepared through a solvothermal reaction using the as-synthesized $Fe_3O_4$ particles and TBOT as the precursors and

**Scheme 1. (a) Synthesis of the Flowerlike $Fe_3O_4$@f$TiO_2$ Microspheres with Hierarchical Structure, (b) Magnetic Purification of Phosphoproteins, and (c) Selective Enrichment of Phosphopeptides for MS Analysis Using the $Fe_3O_4$@f$TiO_2$ Affinity Microspheres**

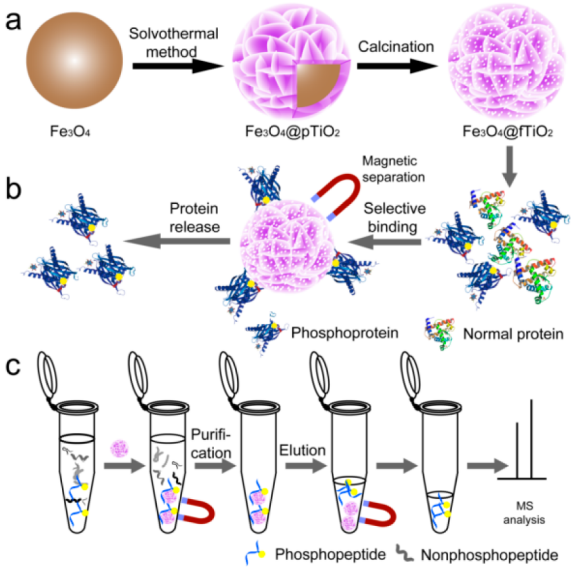


the mixed solution of DMF and IPA as the organic solvent. Then, the hierarchical flowerlike $Fe_3O_4$(and/or $\gamma$-$Fe_2O_3$)@f$TiO_2$ microspheres with meso-/macroporous shell were obtained after the flowerlike $Fe_3O_4$@p$TiO_2$ microspheres were calcined at 400 °C for 2 h in air. To conveniently depict the microspheres, they were still denoted as the $Fe_3O_4$@f$TiO_2$.

Morphologies and structures of the $Fe_3O_4$@p$TiO_2$ microspheres were characterized using scanning electron microscopy (SEM). The precursor $Fe_3O_4$@p$TiO_2$ (Figure 1a and b)

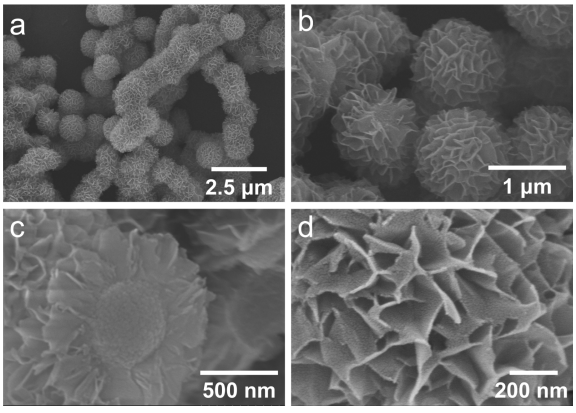


**Figure 1.** SEM images with different magnifications of the flowerlike precursor $Fe_3O_4$@p$TiO_2$ microspheres.

microspheres with an average diameter of about 1 $\mu$m have the flowerlike heterogeneous $TiO_2$ shell. The flower-like $TiO_2$ shell with a thickness of about 270 nm, as revealed in the SEM image of a broken $Fe_3O_4$@p$TiO_2$ microsphere, is composed of many $TiO_2$ nanopetals wrapped around the $Fe_3O_4$ core. Importantly, the petallike $TiO_2$ nanosheets assembled together constructed many macropores with pore size 50−200 nm, which help to avoid the "shadow effect" and the size exclusion effect of the smaller and deeper pores by means of effective mass transport.

High magnification SEM images (Figure 1d and Supporting Information Figure S2a) further demonstrated that the macroporous structure is composed of the cross-linked nanopetals with thickness of about 10 nm, which erectly grew on the surface of the $Fe_3O_4$ microspheres.

Figure 2 shows the SEM and TEM images of the $Fe_3O_4$@$fTiO_2$ microspheres from the calcined $Fe_3O_4$@$pTiO_2$ micro-

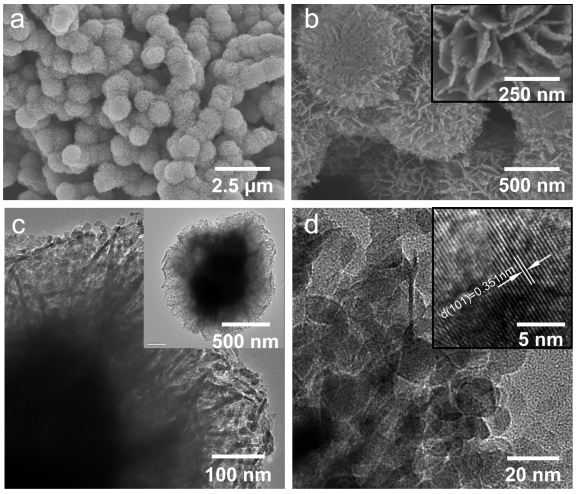


**Figure 2.** (a and b) SEM, (c) TEM, and (d) HRTEM images of the flowerlike $Fe_3O_4$@$fTiO_2$ microspheres with hierarchical structure.

spheres. Compared with the precursor $Fe_3O_4$@$pTiO_2$ microspheres, the flowerlike structures and sizes of the $Fe_3O_4$@$fTiO_2$ microspheres (Figure 2a, b) are almost unchanged. After careful observation and comparison, we found that the nanopetals of the $Fe_3O_4$@$fTiO_2$ microspheres have become very coarse, which may be ascribed to the recrystallization of titania. TEM images of the $Fe_3O_4$@$fTiO_2$ microspheres (Figure 2c) confirm that the $Fe_3O_4$@$fTiO_2$ microspheres are still core–shell structures and the macroporous shells are constructed from curved nanopetals. High-resolution TEM images (Figure 2d) further reveal that the nanopetal composed of numerous nanocrystallites assembled together has many shallow mesopores on it, which can remarkably increase the specific surface area and active sites. In addition, the lattice fringes of these nanocrystallites with a spacing of 0.351 nm (Figure 2d, inset) can be apparently observed, which is in accordance with the spacing of the (101) plane of the anatase phase. Notably, the hierarchical flower-like $TiO_2$ affinity material with unique macropores and shallow mesopores possess low density, high specific surface, and large adsorptive capacity, which can facilitate the transport of target biomolecules, effectively avoid the "shadow effect" and improve the affinity selectivity and efficiency.

The elemental composition and the crystal structure of the $Fe_3O_4$@$fTiO_2$ microspheres can be verified by energy-dispersive X-ray spectrum (EDX), powder X-ray diffraction (XRD), and Fourier-transform infrared (FTIR) spectroscopic analysis. Comparison of EDX spectra between the $Fe_3O_4$@$fTiO_2$ microspheres and the $Fe_3O_4$ particles (as shown in Figure 3a) reveals the existence of the $TiO_2$ shell due to the presence of Ti element in the EDX spectrum of the $Fe_3O_4$@$fTiO_2$ microspheres besides the Fe and O elements. It should be pointed out that the C element in the EDX spectra comes from the conductive tape used to fix the sample.

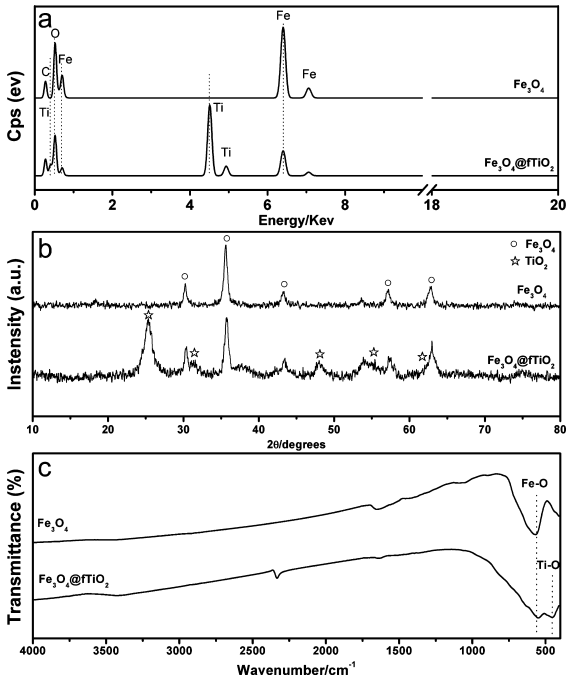


**Figure 3.** (a) EDX spectra, (b) XRD patterns, and (c) FTIR spectra of the $Fe_3O_4$ and the $Fe_3O_4$@$fTiO_2$ microspheres.

Compared with diffraction peaks of the $Fe_3O_4$ particles, diffraction peaks in the XRD pattern of $Fe_3O_4$@$fTiO_2$ microspheres (Figure 3b) can be respectively assigned to the characteristic diffraction peaks from iron oxide ($Fe_3O_4$ and/or $\gamma$-$Fe_2O_3$: JCPDS card no. 75-0449 or 25-1402) and those from the crystalline anatase $TiO_2$ phase (JCPDS card no. 21-1272) (marked asterisk). The XRD result indicates that the $Fe_3O_4$ phase could be entirely or partially transformed into $\gamma$-$Fe_2O_3$ phase after calcination at 400 °C for 2 h in air under protection of the $TiO_2$ coating. It is well-known that it is difficult to distinguish between the two oxides by means of XRD due to their very similar structures. However, in this work, we mainly focused on magnetism of iron oxide for magnetic separation of the target biomolecules.

FTIR spectra of the $Fe_3O_4$ particles and the $Fe_3O_4$@$fTiO_2$ microspheres are shown in Figure 2c. The characteristic absorption peak at around 560 $cm^{-1}$ can be assigned to stretching vibration of Fe–O bonds of the $Fe_3O_4$, while the characteristic absorption peak at around 460 $cm^{-1}$ in FTIR spectra of $Fe_3O_4$@$fTiO_2$ microspheres can be attributed to stretching vibration of Ti–O bonds of the $TiO_2$ shell. In addition, a broad band at around 3400 $cm^{-1}$ can be obviously observed, indicating the existence of many hydroxyls on the surface of $Fe_3O_4$@$fTiO_2$ microspheres. Above results further confirm the formation of the $Fe_3O_4$@$fTiO_2$ microspheres.

**Possible Formation Mechanism of the Flowerlike $Fe_3O_4$@$fTiO_2$ Microspheres.** To understand the formation process of the flowerlike core–shell $Fe_3O_4$@$pTiO_2$ microspheres, time-dependent evolution experiments were carried out and their SEM images were shown in Supporting Information Figure S3. On the basis of the results of time-dependent evolution experiments, a possible formation mechanism is proposed.[38] First, after hydrothermal reaction for 1 h, we found that surface of the $Fe_3O_4$ microspheres has become slightly smooth (Figure S3a), suggesting deposition of titania oligomers. Thus, we speculated the titanium oxyhydrate

species (i.e., titania oligomers), which would play an important role in nucleation of titania, may be produced through alcoholysis reactions or hydrolysis−condensation reactions of TBOT during the initial stage of the solvothermal process.[45] Next, when the reaction time reached 2.5 h, some sparsely thin curved nanosheets grown on the surface of the $Fe_3O_4$ microspheres can be observed (Figure S3b), indicating the emergence of the oriented crystallization growth. This indicated that the titania oligomers continuously grew along the scraggly surface of $Fe_3O_4$ microspheres, finally leading to the formation of many curved and cross-linked together heterogeneous crystalline nuclei. As the reaction time is prolonged from 2.5 to 10 h, the petallike nanosheets cross-linked together grown on the surface of $Fe_3O_4$ microspheres become thicker and denser gradually (Figure S3c), finally resulting in the feature of the flowerlike $TiO_2$ architecture (Figure S3d). Thus, the continuous oriented crystallization growth and self-assembly process of these heterogeneous nuclei of titania could be responsible for the formation of the hierarchical flowerlike $TiO_2$ architectures. Finally, the hierarchical meso-/macroporous $Fe_3O_4$@f$TiO_2$ microspheres were obtained by calcination of the flowerlike $Fe_3O_4$@p$TiO_2$ microspheres after removing the adsorbed water and organic additives (Figure S3e), resulting in high specific surface area and more active sites.

**Porous Structure and Magnetism of the Flowerlike $Fe_3O_4$@f$TiO_2$ Microspheres.** Porous affinity materials are beneficial to increase the affinity selectivity and efficiency of target capturing due to their high surface areas, appropriate pore sizes, and numbers of affinity sites. Nitrogen adsorption−desorption isotherm study was carried out to evaluate the porous structures of the $Fe_3O_4$@f$TiO_2$ microspheres. As shown in Figure 4a, the $N_2$ adsorption−desorption isotherm of the $Fe_3O_4$@f$TiO_2$ exhibits a little hysteresis, thus it could be approximately categorized as type IV with a type-H3 hysteresis loop according to the IUPAC classification,[46] indicating the porous characteristic of the $Fe_3O_4$@f$TiO_2$ microspheres. The conclusion is fully consistent with that of refs 38, 39, and 41. The average Brunauer−Emmett−Teller (BET) specific surface areas and the total pore volume of the $Fe_3O_4$@f$TiO_2$ microspheres are calculated to be 50.45 $m^2/g$ and 0.25 $cm^3/g$, respectively. The pore-size distribution derived from the adsorption branch using the Barrett−Joyner−Halenda (BJH) method (Figure 4a, inset) shows two sets of different pores with sizes concentrating at 2.4 and 15.0 nm for the flowerlike $Fe_3O_4$@f$TiO_2$ microspheres, indicating their hierarchical porous structure. From these results together with the unique morphology observed in the TEM images, it can be concluded that the hierarchical porous structure of the $Fe_3O_4$@f$TiO_2$ microspheres is constructed by the macroporous shell from the stacked nanopetals and the mesoporous nanopetal from the assembled small crystallites. It should be noted that the hierarchical meso-/macroporous shell would contribute to the capture and release of biomolecules of different sizes because the suitable porous structure can improve the affinity efficiency due to existence of more active sites. More importantly, some larger biomolecules like proteins can also be effectively enriched by means of the macroporous structure, which is often restricted by single mesoporous structure.

The magnetic properties of the $Fe_3O_4$ particles as magnetic cores and the $Fe_3O_4$@f$TiO_2$ affinity microspheres were examined at 300 K via a superconducting quantum interface device (SQUID) magnetometer. As revealed in the hysteresis loops (Figure 4b), the microspheres show a strong super-

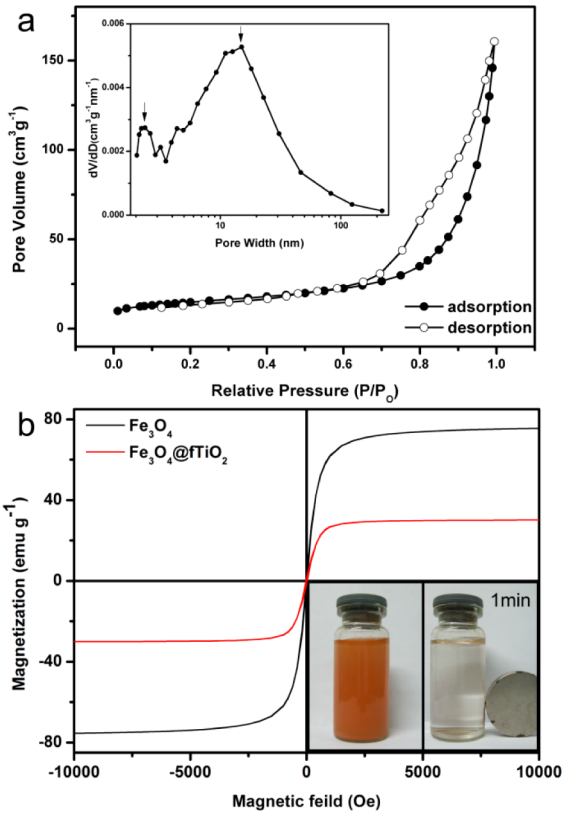


**Figure 4.** (a) $N_2$ adsorption−desorption isotherm and pore size distribution (inset) of the $Fe_3O_4$@f$TiO_2$ microspheres. (b) Magnetic hysteresis loops of the $Fe_3O_4$ and the $Fe_3O_4$@f$TiO_2$ microspheres and dispersion and separation process of the $Fe_3O_4$@f$TiO_2$ microspheres (inset).

paramagnetism at room temperature. The saturation magnetization ($M_s$) values of $Fe_3O_4$ particles and $Fe_3O_4$@f$TiO_2$ microspheres are 75.5 and 30.1 emu/g, respectively. The superparamagnetism of the $Fe_3O_4$@f$TiO_2$ affinity microspheres is beneficial to the rapid and convenient separation. They can be separated from the mixture within 1 min by applying an external magnetic field and rapidly and easily dispersed by shaking after removing the magnetic field (as shown in Figure 4b inset). The result reveals that the affinity microspheres possess the good magnetic response and can meet the requirement of the bioseparation application.

**Selective Binding and Magnetic Separation of Phosphoproteins.** To evaluate adsorption capacity of the $Fe_3O_4$@f$TiO_2$ microspheres for target proteins, $\beta$-casein, and BSA were used as model proteins. As illustrated in Scheme 1b, the affinity microspheres were first incubated with the protein solution for affinity and then separated from the supernatant by a magnet (Scheme 1b). The adsorption capacity of the $Fe_3O_4$@f$TiO_2$ microspheres for model proteins with various concentrations (0.2−1.0 mg/mL) is shown in Supporting Informaiton Figure S4. The adsorption capacities of the $Fe_3O_4$@f$TiO_2$ microspheres for the $\beta$-casein and BSA (1 mg/mL) are 141.4 and 31.1 mg/g, respectively. This indicates that the $Fe_3O_4$@f$TiO_2$ microspheres have larger adsorption efficiency to the phosphoprotein ($\beta$-casein) than that to the nonphosphoprotein (BSA). Compared with commercial $TiO_2$ microspheres, the adsorption capacity of the $Fe_3O_4$@f$TiO_2$ microspheres for phosphoprotein is superior to that of the commercial $TiO_2$ microspheres in our experimental condition obviously.

To further evaluate selectivity of the $Fe_3O_4$@f$TiO_2$ microspheres for phosphoproteins, a complex protein mixture containing one kind of phosphoprotein ($\beta$-casein 23.8 kDa) and three kinds of nonphosphoproteins (myoglobin 16.7 kDa; horseradish peroxidase 42.9 kDa; and BSA 66.1 kDa) was used. The experiments were performed by incubating the $Fe_3O_4$@f$TiO_2$ microspheres with the protein mixture, separating by a magnet, washing off the nonspecifically bound proteins, and eluting the phosphoproteins. The original and residual protein mixture solution and the purified phosphoproteins were then analyzed by MALDI-TOF MS. Figure 5 shows the successful separation of phosphoproteins from the protein mixture. Apparently, the original protein mixture which contained four proteins of various molecular weights shows multiple peaks (Figure 5a), and the signal of $\beta$-casein was very poor due to the low concentration and the suppression of abundant nonphosphoproteins. However, after treatment with the $Fe_3O_4$@f$TiO_2$ affinity materials, only the peaks of three nonphosphoproteins in the residual protein mixture solution can be detected (Figure 5b), indicating $\beta$-casein has be selectively adsorbed by the $Fe_3O_4$@f$TiO_2$ microspheres. In contrast, only the peaks of $\beta$-casein with a strong intensity and a high S/N ratio can be easily detected and no nonphosphoprotein peak can be observed for the captured proteins which were purified and released before MS detection (Figure 5c), indicating that the $Fe_3O_4$@f$TiO_2$ microspheres are effective for the purification and enrichment of phosphoproteins. For comparison, an enrichment test was also performed using commercial $TiO_2$ particles as a substitute for the $Fe_3O_4$@f$TiO_2$ microspheres under the same experimental conditions except centrifugal separation. As shown in Figure 5d, although the phosphoprotein can be enriched effectively, a weak peak of myoglobin can also be observed (Figure 5d). The above results demonstrate the advantages of the $Fe_3O_4$@f$TiO_2$ microspheres in the selective purification and enrichment of the phosphoproteins from the complicate protein mixture.

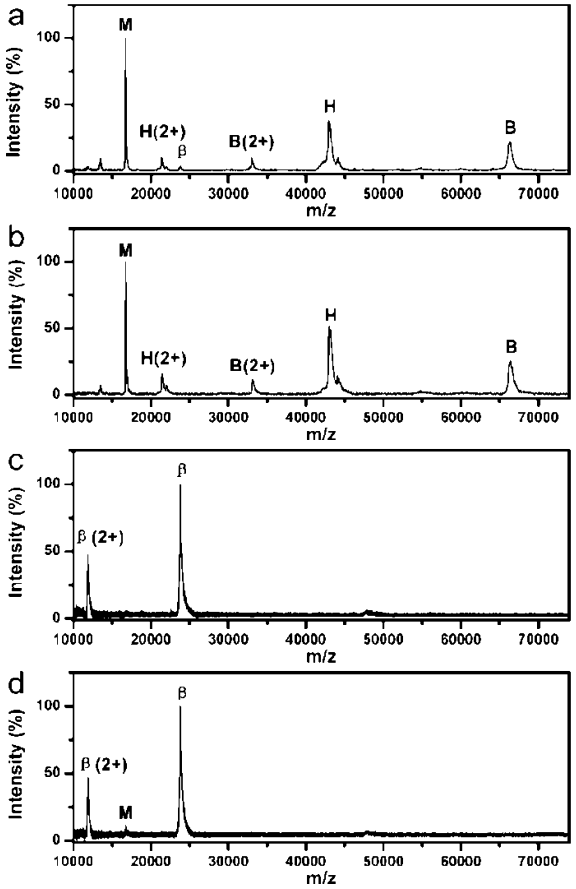


**Figure 5.** MALDI-TOF mass spectra of (a) the original protein mixture before enrichment by the $Fe_3O_4$@f$TiO_2$ microspheres, (b) the residual protein mixture after enrichment by the $Fe_3O_4$@f$TiO_2$ microspheres, (c) the phosphoproteins enriched from the protein mixture by the $Fe_3O_4$@f$TiO_2$ microspheres, and (d) the proteins enriched from the protein mixture by the commercial $TiO_2$ microspheres. "M", "$\beta$", "H", and "B" indicate myoglobin, $\beta$-casein, horseradish peroxidase, and BSA, respectively. "$\beta$(2+)", "H(2+)", and "B(2+)" represent the doubly charged ions of the $\beta$-casein, horseradish peroxidase, and BSA, respectively.

**Selective Enrichment of Low-Abundance Phosphopeptides.** $\beta$-Casein digest, a digest mixture of BSA and $\beta$-casein, and the pristine human serum were used to investigate the effectiveness of the $Fe_3O_4$@f$TiO_2$ microspheres for enrichment of phosphopeptides. As shown in Scheme 1c, the phosphopeptides not only can be enriched by the affinity sites of outer surface of the $TiO_2$ shell, but also can be enriched by the affinity sites inside the porous $TiO_2$ nanopetals due to easy permeation of peptides through the macropores. Meanwhile, the "shadow effect" could be prevented when the enriched phosphopeptides release from the pores. Therefore, high selectivity and affinity efficiency for phosphopeptide enrichment can be obtained by taking advantage of the high specific surface area of the porous structure.

$\beta$-Casein is a common model phosphoprotein, and its tryptic digest contains three phosphopeptides with molecular masses of 2061.8, 2556.0. and 3122.2 Da, respectively. Supporting Information Table S1 lists the molecular masses and corresponding sequences of the enriched phosphopeptides. Figure 6 shows the MALDI mass spectra of the diluted $\beta$-casein digest before and after enrichment by the $Fe_3O_4$@f$TiO_2$ affinity microspheres. Apparently, a few nonphosphopeptides can be detected before enrichment using the affinity microspheres, while phosphopeptides almost cannot be observed due to the low concentration and ionization efficiency (Figure 6a). However, three expected phosphopeptides (marked with

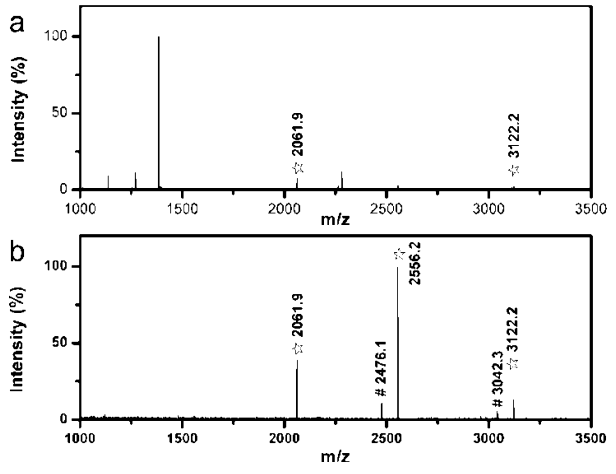


**Figure 6.** MALDI mass spectra of (a) $\beta$-casein digest ($10^{-7}$ M) and (b) $\beta$-casein digest ($10^{-7}$ M) after enrichment with the $Fe_3O_4$@f$TiO_2$ affinity microspheres. "☆" and "#" indicate phosphorylated peptides and their dephosphorylated counterparts, respectively.

"☆") with strong intensity and free from disturbances of nonphosphopeptides after enrichment were evidently detected (Figure 6b). In addition, the dephosphorylated phosphopeptide MS peaks (marked with "#") were also observed. Above results indicate that $Fe_3O_4$@f$TiO_2$ affinity microspheres can selectively capture the phosphopeptides. To evaluate the sensitivity of the used $Fe_3O_4$@f$TiO_2$ affinity microspheres for enrichment of phosphopeptides, we applied the affinity microspheres to enrich the phosphopeptides from $\beta$-casein digest with different concentrations ($5 \times 10^{-8}$, $5 \times 10^{-9}$, and $5 \times 10^{-10}$ M). The experiment results show that the ion signals from the phosphopeptides can still be detected in concentration of low to $5 \times 10^{-10}$ M, which indicates the high detection sensitivity of $Fe_3O_4$@f$TiO_2$ affinity microspheres (Supporting Information Figure S5).

To further evaluate the selectivity, the $Fe_3O_4$@f$TiO_2$ microspheres were used to capture phosphopeptides from a more complex peptide mixture consisting of $\beta$-casein and BSA with different molar ratio ($\beta$-casein:BSA = 1:100, 1:500, 1:1000). For comparison, the precursor $Fe_3O_4$@p$TiO_2$ microspheres without calcination and commercial $TiO_2$ microspheres were also used to enrich the protein mixture. Figure 7a shows

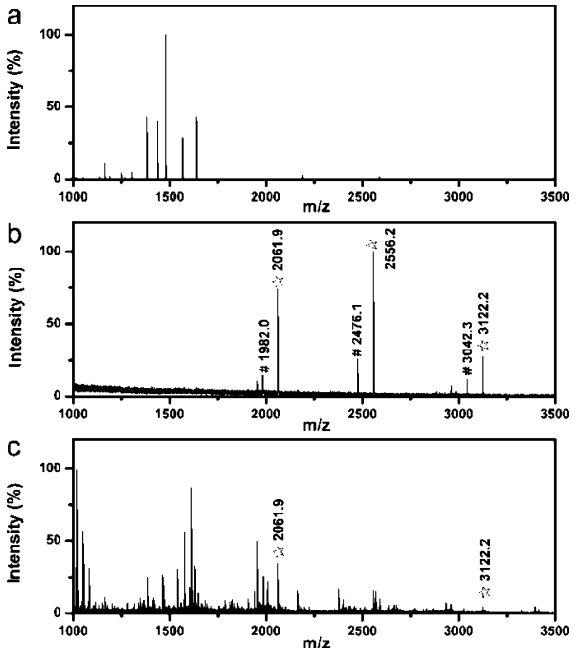


**Figure 7.** (a) MALDI-TOF MS of the tryptic digest mixture of $\beta$-casein and BSA (molar ratio 1:100). MALDI-TOF mass spectra of the tryptic digest mixture of $\beta$-casein and BSA (molar ratio 1:1000) after enrichment with (b) the $Fe_3O_4$@f$TiO_2$ affinity microspheres and (c) the commercial $TiO_2$ microspheres, respectively. "☆" and "#" indicate phosphorylated peptides and their dephosphorylated counterparts, respectively.

the MALDI mass spectrum of the tryptic digestion of $\beta$-casein and BSA at the molar ratio of 1:100 without enrichment. No phosphopeptides can be detected in the mass spectrum owing to the interference of large amounts of nonphosphopeptides. However, three expected phosphopeptides with strong intensities and high S/N ratio are easily detected after enrichment using the $Fe_3O_4$@f$TiO_2$ affinity microspheres (Supporting Information Figure S6). The further experimental result indicates that the phosphopeptides after enrichment using the $Fe_3O_4$@f$TiO_2$ affinity microspheres can still be detected with a clean background, even though the molar ratio of original phosphoprotein to nonphosphoprotein is low to 1:1000 (Figure 7b). To the best of our knowledge, this selectivity is much better than that of most reported $TiO_2$ affinity materials in our experimental condition.[26,29,47] Although the three target phosphopeptides can be detected after enrichment using the precursor $Fe_3O_4$@p$TiO_2$ microspheres, some nonphosphopeptides were also detected (Supporting Information Figure S7a). Some residual organic molecules adsorbed on the surface of the microspheres could be responsible for the phenomenon, which would interfere with the selectivity of the affinity microspheres. For the commercial $TiO_2$ microspheres, only two phosphopeptides as well as many apparent interference signals are detected after enrichment using the commercial $TiO_2$ microspheres (Figure S7b). Although the selective enrichment of phosphopeptide is effective at the low molar ratio of phosphoprotein to nonphosphoprotein, when the molar ratio of original phosphoprotein to nonphosphoprotein is low to 1:1000, only two phosphopeptide peaks with weak intensity and low S/N ratio can be detected, and the dominant MS peaks are all nonphosphopeptides (Figure 7c). Obviously, the great improvement of the selectivity of $Fe_3O_4$@f$TiO_2$ affinity microspheres for phosphopeptide enrichment can be attributed to the unique porous structure of the $Fe_3O_4$@f$TiO_2$ microspheres.

To confirm the enrichment effectiveness for the real biosamples, the $Fe_3O_4$@f$TiO_2$ affinity microspheres were further applied to capture phosphopeptides from human serum. Human serum contains some endogenous phosphopeptides, which might be used as biomarkers for diagnostic and therapeutic methods.[48,49] However, the serum also contains inorganic salts and abundant proteins, as well as a large amount of nonphosphopeptides which seriously interfere with the detection of target phosphopeptides. Figure 8a shows the mass spectrum of the diluted human serum before treatment using the affinity microspheres. Only a few nonphosphopeptides can be detected, because the MS signals of phosphopeptides were severely suppressed and disturbed by the salts and other contaminants in serum. However, three phosphopeptides were successfully detected with clean background at a mass range of 1000−3500 Da (Figure 8b), and no nonphosphopeptide was detected. Supporting Information Table S2 lists the molecular masses and corresponding sequences of the enriched phosphopeptides. By comparison, after enrichment using the commercial $TiO_2$ microspheres, only two phosphopeptides can be detected with low intensity and S/N ratio, and the signals of nonphosphopeptides dominate the whole MS spectrum (Figure 8c). Above results clearly demonstrate that the flowerlike porous $Fe_3O_4$@f$TiO_2$ affinity materials hold great potential for the selective enrichment of phosphorylated proteins/peptides from complex biological samples.

## CONCLUSION

The $Fe_3O_4$@f$TiO_2$ multifunctional affinity microspheres prepared by a facile solvothermal synthesis consist of magnetic cores and flowerlike hierarchical meso-/macroporous $TiO_2$ shells. The unique $TiO_2$ shell structure with large specific surface area not only can markedly improve the selectivity and sensitivity for enrichment of the phosphorylated proteins/peptides from complex biosamples, but also can effectively increase mass transport and prevent the "shadow effect". The fast magnetic response of the superparamagnetism of the

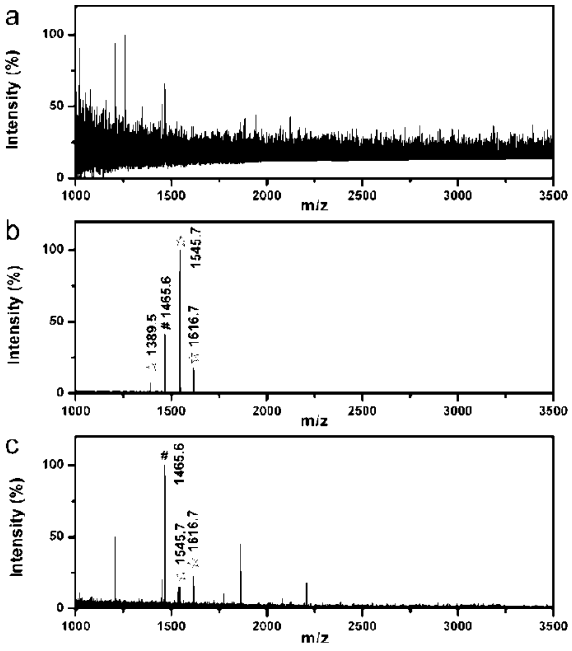


**Figure 8.** (a) MALDI-TOF MS of the diluted human serum solution before enrichment. MALDI-TOF mass spectra of the diluted human serum solution after enrichment with (b) the $Fe_3O_4$@f$TiO_2$ affinity microspheres and (c) the commercial $TiO_2$ microspheres, respectively. "☆" and "#" indicate phosphorylated peptides and their dephosphorylated counterparts, respectively.

$Fe_3O_4$@f$TiO_2$ affinity microspheres also can realize the rapid and convenient separation. Meanwhile, it can be expected that the $Fe_3O_4$@f$TiO_2$ multifunctional affinity materials can be extended to selective enrichment of other phosphate-containing biomolecules. Therefore, this work will be highly beneficial for future applications in the isolation and identification of biomolecules, in particular, low-abundance phosphopeptide biomarkers.

## ■ ASSOCIATED CONTENT

### Ⓢ Supporting Information

More sample characterization (SEM) as well as details of the MS analysis. This material is available free of charge via the Internet at http://pubs.acs.org.

## ■ AUTHOR INFORMATION

### Corresponding Author

*E-mail: zjl@ciac.jl.cn.

### Notes

The authors declare no competing financial interest.

## ■ ACKNOWLEDGMENTS

This work was supported by the National Natural Science Foundation of China (NNSFC) (Grant no. 20871083 and 21171161).

## ■ REFERENCES

(1) Lykourinou, V.; Chen, Y.; Wang, X.-S.; Meng, L.; Hoang, T.; Ming, L.-J.; Musselman, R. L.; Ma, S. *J. Am. Chem. Soc.* **2011**, *133*, 10382−10385.
(2) Shao, M.; Ning, F.; Zhao, J.; Wei, M.; Evans, D. G.; Duan, X. *J. Am. Chem. Soc.* **2011**, *134*, 1071−1077.
(3) Xuan, S.; Wang, F.; Gong, X.; Kong, S.-K.; Yu, J. C.; Leung, K. C.-F. *Chem. Commun.* **2011**, *47*, 2514−2516.
(4) Xiong, H. M.; Guan, X. Y.; Jin, L. H.; Shen, W. W.; Lu, H. J.; Xia, Y. Y. *Angew. Chem. Int. Ed.* **2008**, *47*, 4204−4207.
(5) Zhou, Z.; Taylor, R. N. K.; Kullmann, S.; Bao, H.; Hartmann, M. *Adv. Mater.* **2011**, *23*, 2627−2632.
(6) Guo, Y.; Deng, L.; Li, J.; Guo, S.; Wang, E.; Dong, S. *ACS Nano* **2011**, *5*, 1282−1290.
(7) Lee, J.-H.; Lee, K.; Moon, S. H.; Lee, Y.; Park, T. G.; Cheon, J. *Angew. Chem. Int. Ed.* **2009**, *48*, 4174−4179.
(8) Lee, I. S.; Lee, N.; Park, J.; Kim, B. H.; Yi, Y.-W.; Kim, T.; Kim, T. K.; Lee, I. H.; Paik, S. R.; Hyeon, T. *J. Am. Chem. Soc.* **2006**, *128*, 10658−10659.
(9) Joshi, S.; Ghosh, I.; Pokhrel, S.; Mädler, L.; Nau, W. M. *ACS Nano* **2012**, *6*, 5668−5679.
(10) Peng, L.; Mendelsohn, A. D.; LaTempa, T. J.; Yoriya, S.; Grimes, C. A.; Desai, T. A. *Nano Lett.* **2009**, *9*, 1932−1936.
(11) Ashman, K.; López Villar, E. *Clin. Translat. Oncol.* **2009**, *11*, 356−362.
(12) Domenico, F. D.; Sultana, R.; Barone, E.; Perluigi, M.; Cini, C.; Mancuso, C.; Cai, J.; Pierce, W. M.; Butterfield, D. A. *J. Proteom.* **2011**, *74*, 1091−1103.
(13) Swami, M. *Nat. Rev. Cancer* **2010**, *10*, 597−597.
(14) Hanash, S. M.; Pitteri, S. J.; Faca, V. M. *Nature* **2008**, *452*, 571−579.
(15) Cass, S. M. F.; Tepe, J. J. *Curr. Signal Transduction Ther.* **2011**, *6*, 113−140.
(16) Sun, Z.; Hamilton, K. L.; Reardon, K. F. *J. Molec. Cell. Cardiol.* **2012**, *53*, 354−368.
(17) Paradela, A.; Albar, J. P. *J. Proteome Res.* **2008**, *7*, 1809−1818.
(18) Gao, M.; Deng, C.; Zhang, X. *Exp. Rev. Proteom.* **2011**, *8*, 379−390.
(19) Beltran, L.; Cutillas, P. *Amino Acids* **2012**, *43*, 1−16.
(20) Lu, Z.; Ye, M.; Li, N.; Zhong, W.; Yin, Y. *Angew. Chem. Int. Ed.* **2010**, *49*, 1862−1866.
(21) Zhao, L.; Qin, H.; Hu, Z.; Zhang, Y.; Wu, R. a.; Zou, H. *Chem. Sci.* **2012**, *3*, 2828−2838.
(22) Leitner, A. *Trac-Trend Anal. Chem.* **2010**, *29*, 177−185.
(23) Thingholm, T. E.; Jorgensen, T. J.; Jensen, O. N.; Larsen, M. R. *Nat. Protoc.* **2006**, *1*, 1929−1935.
(24) Wu, J. H.; Li, X. S.; Zhao, Y.; Gao, Q.; Guo, L.; Feng, Y. Q. *Chem. Commun.* **2010**, *46*, 9031−9033.
(25) Lu, Z.; Duan, J.; He, L.; Hu, Y.; Yin, Y. *Anal. Chem.* **2010**, *82*, 7249−7258.
(26) Wan, J.; Qian, K.; Qiao, L.; Wang, Y.; Kong, J.; Yang, P.; Liu, B.; Yu, C. *Chem.—Eur. J.* **2009**, *15*, 2504−2508.
(27) Xu, B.; Zhou, L.; Wang, F.; Qin, H.; Zhu, J.; Zou, H. *Chem. Commun.* **2012**, *48*, 1802−1804.
(28) Han, L.; Shan, Z.; Chen, D.; Yu, X.; Yang, P.; Tu, B.; Zhao, D. *J. Colloid Interface Sci.* **2008**, *318*, 315−321.
(29) Xu, X.; Deng, C.; Gao, M.; Yu, W.; Yang, P.; Zhang, X. *Adv. Mater.* **2006**, *18*, 3289−3293.
(30) Cheng, G.; Zhang, J. L.; Liu, Y. L.; Sun, D. H.; Ni, J. Z. *Chem.—Eur. J.* **2012**, *18*, 2014−2020.
(31) Qin, H.; Gao, P.; Wang, F.; Zhao, L.; Zhu, J.; Wang, A.; Zhang, T.; Wu, R. a.; Zou, H. *Angew. Chem. Int. Ed.* **2011**, *50*, 12218−12221.
(32) Liu, S.; Chen, H.; Lu, X.; Deng, C.; Zhang, X.; Yang, P. *Angew. Chem. Int. Ed.* **2010**, *49*, 7557−7561.
(33) Zhou, H.; Xu, S.; Ye, M.; Feng, S.; Pan, C.; Jiang, X.; Li, X.; Han, G.; Fu, Y.; Zou, H. *J Proteome Res.* **2006**, *5*, 2431−2437.
(34) Kim, J.; Piao, Y.; Lee, N.; Park, Y. I.; Lee, I.-H.; Lee, J.-H.; Paik, S. R.; Hyeon, T. *Adv. Mater.* **2010**, *22*, 57−60.
(35) Cheng, G.; Liu, Y. L.; Wang, Z. G.; Zhang, J. L.; Sun, D. H.; Ni, J. Z. *J. Mater. Chem.* **2012**, *22*, 21998−22004.
(36) Cheng, G.; Liu, Y. L.; Zhang, J. L.; Sun, D. H.; Ni, J. Z. *Anal. Bioanal. Chem.* **2012**, *404*, 763−770.
(37) Deng, Y.; Qi, D.; Deng, C.; Zhang, X.; Zhao, D. *J. Am. Chem. Soc.* **2008**, *130*, 28−29.
(38) Tao, Y.-g.; Xu, Y.-q.; Pan, J.; Gu, H.; Qin, C.-y.; Zhou, P. *Mater. Sci. Eng.: B* **2012**, *177*, 1664−1671.

(39) Chen, J. S.; Liu, H.; Qiao, S. Z.; Lou, X. W. *J. Mater. Chem.* **2011**, *21*, 5687−5692.
(40) Zhu, J.; Wang, S.-H.; Bian, Z.-F.; Cai, C.-L.; Li, H.-X. *Res. Chem. Intermed.* **2009**, *35*, 769−777.
(41) Zhu, T. J.; Li, J.; Wu, Q. S. *ACS Appl. Mater. Interfaces* **2011**, *3*, 3448−3453.
(42) Li, W.; Deng, Y.; Wu, Z.; Qian, X.; Yang, J.; Wang, Y.; Gu, D.; Zhang, F.; Tu, B.; Zhao, D. *J. Am. Chem. Soc.* **2011**, *133*, 15830−15833.
(43) Chen, J. S.; Chen, C.; Liu, J.; Xu, R.; Qiao, S. Z.; Lou, X. W. *Chem. Commun.* **2011**, *47*, 2631−2633.
(44) Cheng, G.; Zhang, J. L.; Liu, Y. L.; Sun, D. H.; Ni, J. Z. *Chem. Commun.* **2011**, *47*, 5732−5734.
(45) Tian, G.; Chen, Y.; Zhou, W.; Pan, K.; Tian, C.; Huang, X.-r.; Fu, H. *CrystEngComm* **2011**, *13*, 2994−3000.
(46) Pierotti, R.; Rouquerol, J. *Pure Appl. Chem.* **1985**, *57*, 603−619.
(47) Li, Y.; Wu, J.; Qi, D.; Xu, X.; Deng, C.; Yang, P.; Zhang, X. *Chem. Commun.* **2008**, 564−566.
(48) Hu, L.; Zhou, H.; Li, Y.; Sun, S.; Guo, L.; Ye, M.; Tian, X.; Gu, J.; Yang, S.; Zou, H. *Anal. Chem.* **2009**, *81*, 94−104.
(49) Zhu, J.; Wang, F.; Cheng, K.; Song, C.; Qin, H.; Hu, L.; Figeys, D.; Ye, M.; Zou, H. *J. Proteom.* **2012**, *78*, 389−397.